Fragmentation of thin films bonded to solid substrates: Simulations and a mean-field theory

Kevin M. Crosby and R. Mark Bradley
Department of Physics, Colorado State University, Fort Collins, Colorado 80523
(Received 16 October 1996)

We perform simulations of crack growth in a brittle-elastic two-dimensional film bonded to a rigid substrate and subjected to an isotropic tensile stress. We find that the resulting fracture patterns can be classified according to the applied tensile stress. For a significant range of stresses, the crack interactions are extremely short range. The resulting fracture patterns are independent of stress and depend only on the initial distribution of crack nuclei. In this regime, the fracture process is well described by a fragmentation model in which a random distribution of seeds nucleates pairs of oppositely directed rays which grow until encountering other rays. Using a mean-field approach, we obtain approximate analytical results for this model which compare well with both the simulations of the fragmentation model, and with the fracture simulation results. Our approach is extensible to other models of fracture, and where numerical results exist in the literature, our mean-field solutions agree well with them. [S1063-651X(97)02705-0]

PACS number(s): 03.40.−t, 61.43.Bn, 62.20.Mk, 81.30.Kf

I. INTRODUCTION

The process of fragmentation has been the subject of much interest recently as a number of authors have obtained exact solutions for a class of fragmentation models [1–6]. These models have been proposed in the context of many important physical and chemical phenomena. These include explosions [7], atomic collision cascades [8], droplet breakup [9], and polymer degradation [10]. A basic premise of these models is that as the fragmentation process proceeds, the fragments split independently of one another. Fragments continue to split independently in time. This permits the introduction of linear rate equations to describe the evolution of the fragment size distribution. Solutions to these ''fragmentation equations'' for several fragmentation rules are now well established.

There are fragmentation phenomena, however, which are not well described by linear rate equations. Fracture of elastic solids typically initiates from scattered defects in the medium which nucleate cracks upon exposure to a supercritical tensile stress. The nucleation of cracks is heterogeneous in this case. If the elastic solid is a thin film bonded to a solid substrate, the final structure resembles a patchwork of polygonal islands of undamaged film bounded by cracks. If the film is a conductor and the substrate an insulator, the film undergoes a conductor-insulator transition upon sufficient fragmentation.

Tensile fracture of real thin film materials is a significant obstacle to reliability engineering of many important technologies. Very large scale integrated circuitry (VLSI) relies in part on the integrity of thin metal and dielectric films which are often under large tensile stresses applied by their substrates. The deposition process is often responsible for the high tensile stress. For example, metal-vapor deposition frequently produces films with high tensile stresses which are then used in optical applications [11]. Epitaxial alkaline earth fluoride films are candidate materials for use as passivating layers on semiconductors and these films are also under high intrinsic tensile stress [12].

In this paper we present the results of computer simulations of tensile fracture in thin films bonded to solid substrates. The simulations show that a fragmentation model, in which the crack tip velocities are constant in time, is a good approximation to the actual, more complicated dynamics for a significant range of stresses. This intermediate stress regime is characterized by final film surface configurations which can be reproduced by application of a set of simple, stress-independent crack growth rules to the distribution of initial defects. We numerically investigate such a model and find crack length distribution functions which compare well with the analogous distribution functions obtained from the fracture simulations.

For stresses above the intermediate regime, we find increasingly complex crack interactions which lead to stress-dependent final states. We also propose a mean-field description of a generic, heterogeneous fragmentation process and analyze its properties in the context of the tensile-fracture simulations. We show that our solution can be specialized to describe the properties of related models of fragmentation, and that where numerical estimates of fragment length distributions exist in the literature, our solutions agree quite well with them.

II. BRITTLE-ELASTIC THIN FILM MODEL

Our model is a deterministic central-force lattice model which consists of a triangular array of masses (the film) connected by Hookean bonds to each other and to a planar triangular array representing the substrate. Each mass in the film is anchored to three substrate sites by a tripod of bonds. The number of sites along an edge of the film defines the linear dimension L of the lattice, where we have set the initial lattice spacing to 1.0.

We work with $L\times L$ lattices, so that there are L^2 sites in the film layer. We choose the substrate to have $L+1$ sites along an edge which ensures that the edge sites in the film are fully anchored to the substrate. There are $(L-1)(3L-1)$ bonds in the film and $3L^2$ adhesive bonds. Taken together, the film and substrate form a rhombus consisting of two adjacent (111) planes of an fcc lattice (Fig. 1).

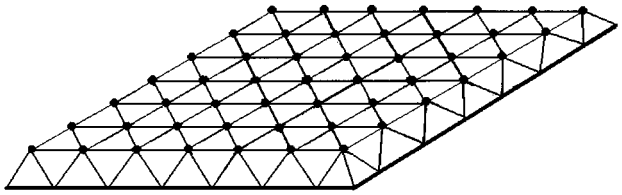

FIG. 1. Geometry of film and substrate. The fixed substrate sites are not shown.

A film site i with mass m obeys the equation of motion

$$m\ddot{\vec{x}}_i = -b\dot{\vec{x}}_i + \sum_{j\neq i} \vec{F}(\vec{x}_i - \vec{x}_j), \tag{1}$$

where we consider nearest-neighbor interactions only, so that the sum on j is over nine neighbors (six in-plane neighbors and three adhesively bonded substrate neighbors). The displacement from equilibrium for the site i is $\vec{x}_i$. The quantity b is a phenomenological damping coefficient. The magnitude of dissipative losses is characterized by the quantity $\eta \equiv b/m$. In the simulations reported here, we consider purely dissipative dynamics where $\eta=\infty$. The force term in Eq. (1) represents the Hookean interaction with ''spring constant'' k_{ij}, i.e., $\vec{F}(\vec{x}_i-\vec{x}_j) = -k_{ij}(\vec{x}_i-\vec{x}_j)$. We choose k_{ij} to have the same value k for all unbroken bonds in the lattice, and we set $k_{ij}=0$ for broken bonds. The value of k sets the scale for the elastic properties of the lattice and dictates the choice of the time step when Eq. (1) is integrated numerically.

The bonds which connect the masses to each other have temperature dependent natural lengths with thermal expansion coefficients α_{ij}. We set all α_{ij}'s for the film and adhesive bonds to the same value α_f, and all α_{ij}'s for the substrate bonds to zero. This results in a rigid substrate, which is a plausible assumption if the film is much thinner than its substrate, as is usually the case. A state of tensile stress is introduced by requiring that $\alpha_f>0$ and reducing the temperature of the lattice incrementally to some final value. In this way, the film layer's contraction is imposed by the rigid substrate. The bonds in the film layer break irreversibly when they bear a strain in excess of a threshold value ϵ_c which we have chosen to be 0.02 for the simulations reported here. The adhesive bonds are not permitted to break. The applied stress in the film in the absence of any broken bonds is given by

$$\sigma_0 = \frac{E_0}{(1-\nu)}\,\alpha_f|\Delta T|, \tag{2}$$

where E_0 and ν are, respectively, the Young's modulus and Poisson ratio of the undamaged film and $|\Delta T|$ is the temperature drop. It is straightforward to show that $E_0=(2/\sqrt{3})k$ and $\nu=1/3$ for a two-dimensional triangular lattice subjected to plane stress. We set a convenient scale for the stress in the simulations by measuring the initial stress in units of $E_0/(1-\nu)$ and temperature in units of $1/\alpha_f$. σ_0 is then numerically equal to the depth of the temperature drop $|\Delta T|$, which is the quantity we control directly. Our simulations span the range $15<\sigma_0\leqslant 100$.

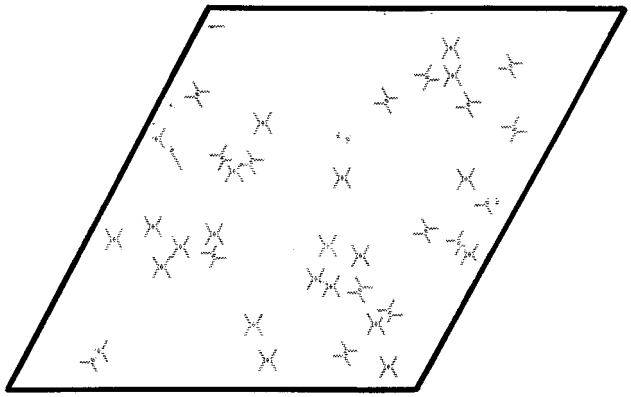

FIG. 2. Film surface shortly after onset of fracture. The simulation parameters are $L=150$, $\gamma=0.01$ and $\sigma_0=27.0$.

III. SIMULATION RESULTS

Initially, a random distribution of defects in the form of broken bonds is present in the film layer. Let γ denote the initial defect density. As the temperature is lowered, bonds contiguous to the initial defects begin to rupture, generating cracks. We have also allowed the initial state to contain a small fraction of adhesive disorder through the presence of randomly placed, broken adhesive bonds. This is thought to mimic the likely imperfect adhesion between real films and their substrates. We observe no substantive change in the fracture dynamics when such dilute adhesive disorder is included. In what follows, we will restrict our attention to the simulations in which there is no adhesive disorder present.

There is a γ-dependent threshold stress $\sigma_m(\gamma)$ for the onset of cracking. For $\sigma_0\geqslant\sigma_m(\gamma)$, the crack tips initially propagate along lattice vectors. Figure 2 shows the film surface after a short time on a lattice of size $L=150$ with $\gamma=0.01$. An obvious feature of Fig. 2 is the appearance of a generic crosslike pattern common to most defects. This feature is a consequence of the symmetries of the lattice. Most defects nucleate a crosslike crack pattern with branch angles of 60° and 120° relative to the initially broken bond.

The depth of the temperature quench dictates the subsequent evolution of the fracture pattern. From simulations over a wide range of stresses, one can identify three types of final states which we label ''incipient,'' ''intermediate,'' and ''strongly interacting'' in reference to the dominant crack dynamics observed in each case. Let $\sigma_i(\gamma)$ represent the values of σ_0 that distinguish these final states, where $i=1$ or 2.

For stresses σ_0 in the range $\sigma_m(\gamma)\leqslant\sigma_0<\sigma_1(\gamma)$ (the incipient regime), there is not enough strain energy in the film to support full fragmentation of the film surface. Most crack tips stop before intersecting other cracks. The film surface is characterized by a scattering of small, isolated crosslike cracks with a small number of longer cracks. That σ_1 is a function of γ can be understood in terms of the decreasing mean distance between defects with increasing γ. Larger defect densities result in a smaller mean distance between crack tips, and therefore, an increased probability of intersection.

For $\sigma_1(\gamma)\leqslant\sigma_0\leqslant\sigma_2(\gamma)$ (the intermediate regime), we find long-time configurations like that shown in Fig. 3. The value of σ_0 for this simulation is 26.5. A significant feature of the pattern shown in Fig. 3 is the absence of intersecting

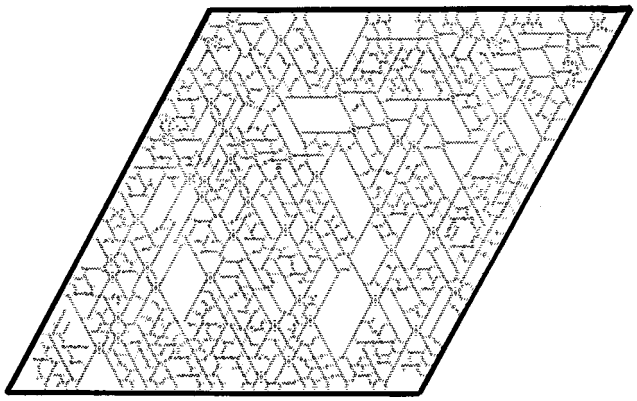

FIG. 3. Final configuration of the film surface for $\sigma_0 = 26.5$ and $\gamma = 0.1$ on a lattice of size $L = 150$. This pattern is typical of those obtained in the intermediate regime.

cracks. Propagating crack tips move in straight lines until they are arrested as they approach other cracks. The crack tip velocities are approximately uniform throughout the film for this choice of σ_0. Crack propagation typically initiates before the target σ_0 is reached. As a result, crack tip velocities increase with time. However, they do so uniformly throughout the film as we show below.

The direct determination of crack tip velocities poses a technical challenge since we must determine the crack branch to which a given broken bond belongs. This procedure is particularly ambiguous in the high density or high stress simulations. For a dilute network, i.e., one in which the defects initially present are far apart on average, a simple algorithm can be implemented which will reliably measure crack lengths. The procedure we adopt is to assign four ''crack paths'' to each defect based on the defect's orientation in the lattice. These paths consist of lists of bonds which lie along the likely paths of the crack branches. As bonds break sequentially along these paths, the crack length per path is recorded as the number of adjacent breaks along the path. In Fig. 4, we show the time evolution of the lengths of 100 randomly chosen crack branches. The simulation parameters are $\gamma = 0.01$ and $\sigma_0 = 27.5$. The lattice size is $L = 80$.

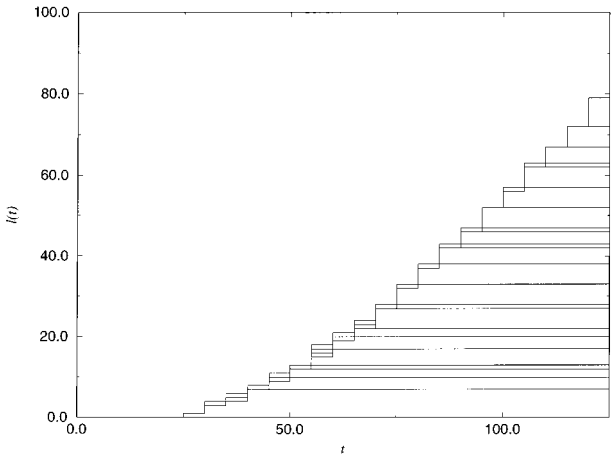

FIG. 4. Crack lengths vs time for 100 randomly selected defects in a film with dilute disorder ($\gamma = 0.01$). The lattice size is $L = 80$ and $\sigma_0 = 27.5$.

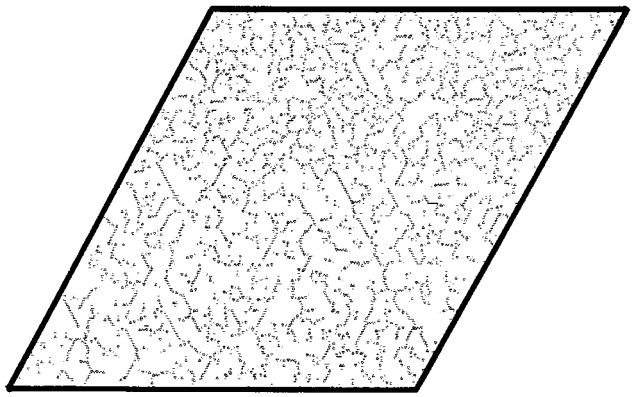

FIG. 5. Final configuration of the film surface for $\sigma_0 = 26.0$ and $\gamma = 0.30$.

Many of the crack branches represented in Fig. 4 evolve identically, resulting in the appearance of a smaller number of trajectories. The near coincidence of all the trajectories before arrest indicates that the cracks propagate with a common velocity. In fact, the variance is everywhere less than 0.5.

This procedure is adequate for $\gamma < 0.2$. For γ greater than about 0.2, the defects are sufficiently close on average that cracks form by bridging the gaps between defects with straight crack segments. The resulting pattern is not a polygonal network of cracks bounding patches of undamaged film, but instead contains long, winding cracks surrounded by inactive defects (Fig. 5).

Sufficiently energetic cracks, however, interact in a complicated way; the velocity of the propagating crack tip dictates whether or not it is arrested by another crack in its path. The tip velocity and direction are complicated functions of the stress field ahead of the crack tip which is modified by the presence of other nearby cracks. These effects are observed in the simulations for σ_0 larger than $\sigma_2(\gamma)$ (the strongly interacting regime). Figure 6 shows a final state fracture pattern with $\sigma_0 = 36.0$. This pattern reflects the more complicated crack interactions of branching and crossing.

There is, of course, some ambiguity in the choice of the σ_i's. While the essential observation is the existence of the three regimes, there are no sharp boundaries in stress be-

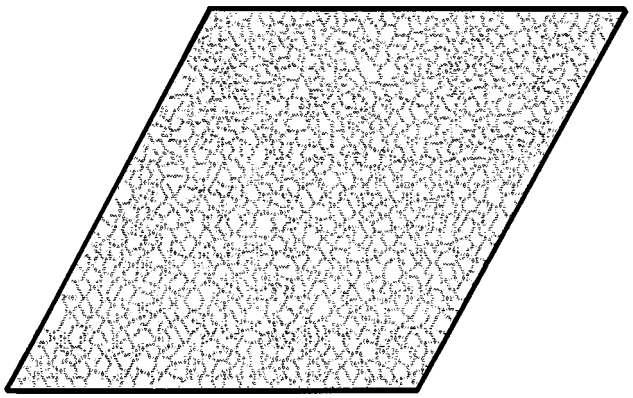

FIG. 6. Final configuration of the film surface for $\sigma_0 = 36.0$ and $\gamma = 0.1$ on a lattice of size $L = 150$. This pattern is typical of those obtained in the strongly interacting regime.

tween them. What is important is the width of the intermediate regime, $\sigma_2(\gamma)-\sigma_1(\gamma)$, which we have chosen to define in the following way. We choose this width to represent the range of σ_0 for which all crack tips terminate upon first encountering another crack tip or boundary. This width is also characterized by the uniformity of the crack tip velocities. For $\gamma \leqslant 0.20$, the width is approximately 18, a significant portion of the total stress range of $15 \leqslant \sigma_0 \leqslant 100$ we have examined. The lower boundary roughly corresponds to σ_m for the range of seed density γ we have explored. For $\sigma_0 > 100$, the crack density is too high to resolve separate cracks in lattices of a reasonable size ($L \leqslant 250$).

The crosslike cracks we observe in our fracture simulations arise from the symmetries of the triangular lattice. We can eliminate this multiple nucleation effect by nucleating correlated defects as follows. For each of the broken bonds initially present in lattice, we break an adjacent bond whose orientation defines the incipient crack's subsequent propagation direction. In this way, defects generate single cracks which grow with equal probability along any of the three lattice vectors.

IV. A HETEROGENEOUS FRAGMENTATION MODEL

For stresses in the intermediate regime, we find only straight, nonintersecting cracks in our simulations. Further, in this intermediate range of σ_0, crack branching is relatively rare and the spread in crack tip velocities is quite small throughout the evolution of the pattern. We can draw an important conclusion from these observations: In the intermediate regime, the final configuration of the film is, to a good approximation, independent of the stress and is a function of the initial distribution of defects alone.

This leads naturally to the description of the fracture process in terms of a fragmentation model which we define by a set of simple rules: Cracks nucleate simultaneously from randomly scattered defects and propagate with constant velocity, stopping upon contact with other cracks. That fracture might be modeled in such a way has been proposed before [13–15]. That it is a fair approximation (at least for a range of tensile stresses), has to our knowledge never before been confirmed. In what follows, we discuss simulations of this fragmentation model and obtain crack length distribution functions which agree well with those obtained from the thin film fracture simulations.

We have carried out simulations on the fragmentation model defined above for the case in which each defect nucleates a pair of oppositely directed crack branches. The orientation of the cracks on the lattice is chosen with equal probability to be one of the three allowed orientations on the triangular lattice. In Fig. 7, we show the crack length distributions obtained from both the fracture simulations (with correlated defects) in the intermediate regime and simulations of the fragmentation model. For both simulations, the initial defect density γ is 0.20. The agreement between the fragmentation and fracture simulations is quite good over the entire range of crack lengths.

We expect that fracture (in the intermediate regime) on the square lattice and off-lattice fracture can be similarly modeled by the fragmentation model. In fact, fragmentation by randomly oriented cracks has been numerically studied

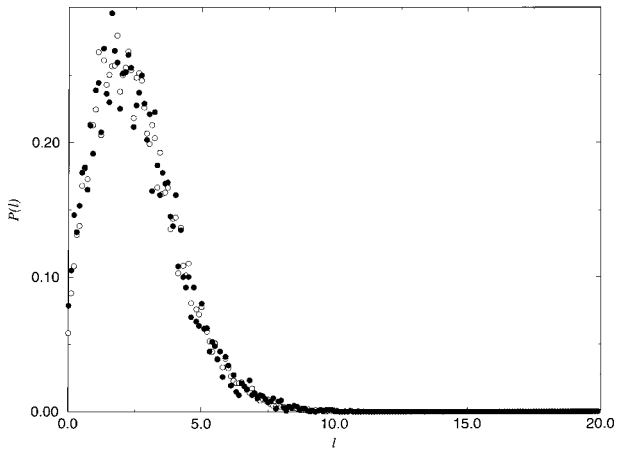

FIG. 7. Ray length probability distributions obtained from fracture (●) and fragmentation (○) simulations with $\gamma = 0.20$. The fracture simulations were carried out with $\sigma_0 = 26.5$ on a lattice of size $L = 150$.

before [14]. Another variation of the fragmentation model has been used to describe martensite growth [16], a phenomenon which bears similarities to square lattice fracture in real materials [12]. In the following sections, we develop a mean-field theory for a general, heterogeneous fragmentation model and compare its properties to these fragmentation simulations and to our own thin film fracture simulations.

V. A MEAN-FIELD THEORY OF HETEROGENEOUS FRAGMENTATION

In this section we obtain approximate expressions for the crack length distribution functions of a generic heterogeneous fragmentation model. We show that our results are applicable to any fragmentation process in which randomly scattered seeds simultaneously nucleate single pairs of oppositely directed rays which propagate with constant velocity until they are stopped by other rays. By appropriate choice of the ray pair orientations, the solutions we obtain can be specialized to describe a variety of previously studied models, as well as the thin film fracture model of Sec. II.

We begin by considering seeds distributed randomly on a plane with seed density γ. At $t = 0$, each seed nucleates a pair of oppositely directed rays each of which grows with the same speed (and with the same speed as all other rays on the plane). The orientation of the ray pair is described by an angular distribution function $D(\theta)$, where $0 \leqslant \theta \leqslant \pi$, which specifies the orientation of the ray pair relative to the x axis. $D(\theta)d\theta$ is the probability of finding a ray with orientation between θ and $\theta + d\theta$. A coordinate system is placed with its origin lying on a seed and with its axes oriented so that the ray pair lies along the x axis. Let x denote the length of the ray lying on the positive x axis after all rays have stopped growing. We now ask for the ray-length distribution function, $\tilde{P}(x)$.

We proceed by defining $F(x_0)$ to be the probability that the ray nucleated at the origin and directed along the positive x axis grows to a length $x \geqslant x_0$. In order for this to occur, there can be no ''blocker'' rays which pass through the x axis between $x = 0$ and $x = x_0$. For each orientation θ, we

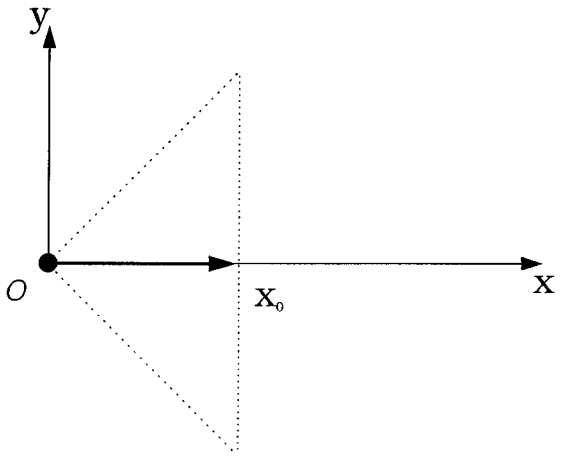

FIG. 8. The region enclosing $A(\pi/2)$ for the special case $D(\theta)=\frac{1}{2}[\delta(\theta)+\delta(\theta-\pi/2)]$ is outlined with dotted lines.

identify a region of area $A(\theta)=x_0^2\sin\theta$ symmetric about the x axis and spanned by the line segment $0\leqslant x\leqslant x_0$. All rays originating within this region which have orientation θ will, if unblocked, intersect the line segment $0\leqslant x\leqslant x_0$ *before* the ray propagating along the x axis does so. To make the construction clear, we consider the special case $D(\theta)=\frac{1}{2}[\delta(\theta)+\delta(\theta-\pi/2)]$ so that each seed nucleates a ray pair with one of two perpendicular orientations with equal probability. $A(\theta=\pi/2)$ is then the area enclosed by the right triangle symmetric about the x axis, with a vertex at the origin, and with base length $2x_0$ (Fig. 8). Any ray which originates within $A(\pi/2)$ *and* which has the orientation $\theta=\pi/2$ has the potential to prevent the ray at the origin from reaching $x=x_0$ and is termed a ''blocker'' ray. Whether it does so depends on the absence of ''blocker-blocker'' rays which in this case must have orientation $\theta=0$ or π and lie within a right triangle with its vertex at the origin of the blocker ray.

For arbitrary θ, $A(\theta)$ is the area enclosed by the dashed lines in Fig. 9. This shape, which is a chevron for $\theta>\pi/2$ and a diamond for $\theta<\pi/2$, has an opening angle 2ω with ω given by

$$\tan\omega=\frac{\sin\theta}{1-\cos\theta},$$

where the principal branch of the tangent function is taken. In what follows, we consider this general case.

We consider a blocker defect with orientation θ nucleated at the point (x,y) to be potent if it grows to a length $x'\geqslant y/\sin\theta$ and has a ray which intersects the line segment $0<x\leqslant x_0$. The geometry is illustrated in Fig. 9.

Let us now make an assumption which amounts to a mean-field type approximation. To proceed with the calculation it is necessary to assume that the blocker defects are statistically independent of one another. That is, given knowledge of the length of one potential blocker, nothing can be said about the lengths of other blockers. This assumption is clearly not valid in general. However, it does appear that the ray length correlations are small, and in fact, vanish in the high density limit. Ultimately, the justification for this approximation will come from the surprising accuracy of the crack length statistics obtained from the theory. We will

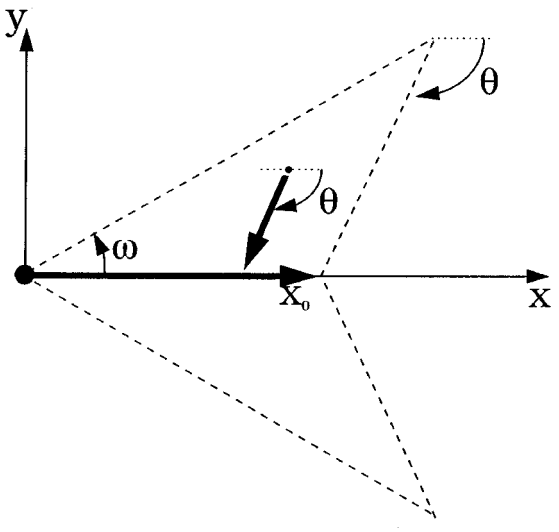

FIG. 9. The region enclosing $A(\theta)$ is outlined with dashed lines. Also shown is the geometry of the ray interactions.

therefore decompose $F(x_0)$ into a product over all points (x,y) and possible orientations θ within the area $A(\theta)$. Each factor in the product then represents the probability that a potent blocker does not exist at the point (x,y). $F(x_0)$ can be formally written as

$$F(x_0)=\prod_{(x,y,\theta)}[1-\Gamma(y,\theta)]. \tag{3}$$

$\Gamma(y,\theta)$ is the probability that a ray nucleates in the area element $dx\,dy$ at (x,y) with orientation θ and is a potent blocker. It is straightforward to show that $\Gamma(y,\theta)=\gamma\,dx\,dy\,d\theta\,D(\theta)F(|y|\csc\theta)$. The product in Eq. (3) is to be taken over all x, y, and θ satisfying the potency conditions

$$|y|\leqslant x_0\sin\theta,$$

$$|y|(\csc\theta-\cot\theta)\leqslant x\leqslant x_0-|y|\cot\theta,$$

and

$$0\leqslant\theta\leqslant\pi.$$

Taking the natural logarithm of both sides of Eq. (3), using the relation $\ln(1-x)\approx -x$ for small x, and converting the resulting triple sum to integrals yields

$$\begin{aligned}\ln F(x_0)&=-\gamma\int_0^{\pi}d\theta\int_{-x_0\sin\theta}^{x_0\sin\theta}dy\int_{|y|(\csc\theta-\cot\theta)}^{x_0-|y|\cot\theta}dx\,D(\theta)\\&\quad\times F(|y|\csc\theta)\\&=-2\gamma\int_0^{\pi}d\theta\int_0^{x_0\sin\theta}dy\,D(\theta)(x_0-y\csc\theta)\\&\quad\times F(y\csc\theta),\end{aligned}$$

where we have made use of reflection symmetry about the x axis. A change of variable $z\equiv y\csc\theta$ results in

$$\ln F(x_0) = -2\gamma I \int_0^{x_0} dz (x_0 - z) F(z) \tag{4}$$

where we have defined $I \equiv \int_0^{\pi} d\theta (\sin\theta) D(\theta)$.

Equation (4) permits an exact solution. Differentiating twice with respect to x_0, we obtain the nonlinear differential equation

$$F(x_0)F''(x_0) - [F'(x_0)]^2 + 2\gamma I [F(x_0)]^3 = 0. \tag{5}$$

Equation (5) can be transformed to a Bernoulli equation [17] and solved by means of an integrating factor. The general solution is

$$F(x_0) = \frac{c_1}{4\gamma I} \operatorname{sech}^2[\tfrac{1}{2}\sqrt{c_1}(x_0 + c_2)],$$

where c_1 and c_2 are constants. We can then get the ray length probability distribution $\widetilde{P}(x)$ from $\widetilde{P}(x) = -dF(x_0)/dx_0|_{x_0 = x}$. Normalizing and requiring that $\widetilde{P}(0) = 0$ results in

$$\widetilde{P}(x) = \sqrt{4\gamma I}\, \frac{\sinh(\sqrt{\gamma I}x)}{\cosh^3(\sqrt{\gamma I}x)}. \tag{6}$$

Equation (6) gives an approximate expression for the distribution of ray lengths arising from a heterogeneous fragmentation process defined by an angular distribution function $D(\theta)$. To facilitate comparison with the numerical data of other fragmentation studies, it is necessary to compute $P(l)$, the distribution function for line segment lengths. Now, a line segment of length l is composed of two rays of length x and $l - x$. The regions in which we might find potent blockers of these oppositely directed rays do not overlap, so their lengths are statistically independent and we can obtain $P(l)$ from

$$P(l) = \int_0^l dx\, \widetilde{P}(x)\widetilde{P}(l - x). \tag{7}$$

The evaluation of the integral in Eq. (7) is straightforward but results in a rather complicated expression for $P(l)$:

$$P(l) = \frac{(y^2 - 1)}{y^3} [y^2(6 - y^2) + (12 - 8y^2)\ln(1 - y^2)], \tag{8}$$

where $y \equiv \tanh(\sqrt{\gamma I} l)$. The expression of Eq. (8) behaves near the origin as l^3, while $\widetilde{P}(x)$ is linear in x for small x. The l^3 behavior of $P(l)$ is consistent with simple probability arguments [16].

Equations (6) and (8) represent the essential results of the mean-field treatment. In the following section we compare these results with the numerical estimates of crack length distribution functions obtained in previously studied fragmentation models.

VI. ACCURACY OF MEAN-FIELD RESULTS

By an appropriate choice of $D(\theta)$, Eq. (8) can be specialized to represent a number of heterogeneous fragmentation models for which numerical estimates of $P(l)$ exist in the literature. In Ref. [16], Rau *et al.* propose a model of martensite growth in which seeds nucleate single line segments simultaneously (in one limit of the model). These grow with constant velocity and with equal probability along one of two perpendicular directions. The numerical estimate of $P(l)$ is fit to a Γ distribution in Ref. [16]. By letting $D(\theta) = \frac{1}{2}[\delta(\theta) + \delta(\theta - \pi/2)]$, the expression (8) can be specialized to represent the segment length distribution of the model of Ref. [16]. Figure 10 shows a plot of $P(l)$ vs the reduced variable $\sqrt{\gamma/2}\, l$ for both the numerical estimate of Ref. [16] and the expression of Eq. (8). The agreement is quite good over the entire range of data. The relative error is most pronounced near the peak of the distribution, where a maximum error of 6.7% is incurred.

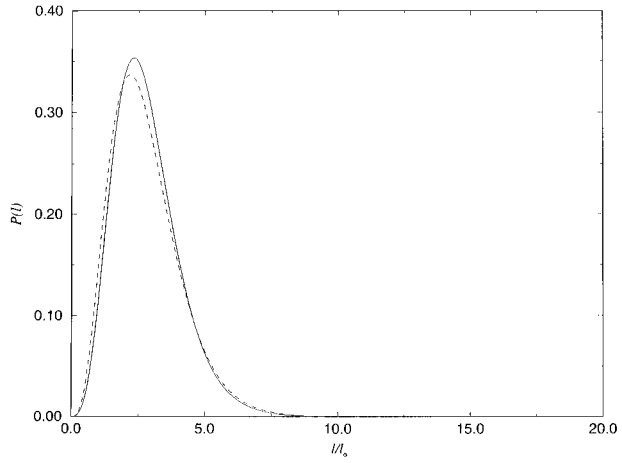

FIG. 10. Line segment probability distribution $P(l)$ vs l/l_0 where $l_0 \equiv \sqrt{2/\gamma}$. The dashed line is the Γ-distribution fit obtained by Rau *et al.* [16].

The mean-field expression for $P(l)$ can be used to obtain expressions for the moments of the distribution which again agree quite well with those obtained from the Γ distribution of Ref. [16]. Computing the moments $M_n \equiv \int_0^{\infty} l^n P(l) dl$ of Eq. (8) is rather awkward. We can however directly obtain the moments, $\widetilde{M}_n$ of the simpler distribution, $\widetilde{P}(x)$ of Eq. (6). A short calculation yields

$$\widetilde{M}_n = 4n(2\gamma)^{-(1/2)n}(1 - 2^{2-n})\Gamma(n)\zeta(n - 1), \tag{9}$$

where $\zeta(n-1)$ is the Riemann zeta function.

To proceed, we note that $P(l)$ is the convolution of $\widetilde{P}(x)$ so that their Laplace transforms, $P(k)$ and $\widetilde{P}(k)$, have the simple relation $P(k) = \widetilde{P}^2(k)$. Now $\widetilde{P}(k) \equiv \int_0^{\infty} \widetilde{P}(x) e^{-kx} dx$, which can be written

$$\widetilde{P}(k) = \sum_{n=0}^{\infty} \frac{(-k)^n}{n!} \widetilde{M}_n.$$

Computing $P(k) = \widetilde{P}^2(k)$, we obtain

$$P(k) = \sum_{n=0}^{\infty} \frac{(-k)^n}{n!} \sum_{m=0}^{n} \binom{n}{m} \widetilde{M}_m \widetilde{M}_{n-m},$$

from which the moments of $P(l)$ are found to be

$$M_n = \sum_{m=0}^{n} \binom{n}{m} \widetilde{M}_m \widetilde{M}_{n-m}. \tag{10}$$

The first two moments obtained from Eq. (10) are $M_1 = 2\sqrt{2/\gamma}$ and $M_2 = 2(2/\gamma)(1+2\ln 2)$ in excellent agreement with the moments obtained from the numerical fit in Ref. [16]. We find a relative error of $\leqslant 3\%$ for the first three moments. The higher-order moments, however, show more pronounced deviations from their numerically estimated counterparts.

In Ref. [14], a model similar in spirit to that of Rau *et al.* is proposed for the fragmentation of a solid due to simultaneous nucleation of cracks. The essential difference between the models is that in the simulations of Ref. [14], defects nucleate single cracks (ray pairs) with random orientations instead of orientations fixed along perpendicular lattice vectors. Again, a Γ distribution is fit to the segment-length distribution. While the uncertainty in the fit parameters is much larger in the work of Ref. [14], we still find that Eq. (8) with $D(\theta) = 1/\pi$ (i.e., with all angles being equally probable) reproduces the Γ-distribution fit with a maximum deviation of 8% between the distributions.

Recently, Birnie and Weinberg presented a model of phase transformation in which anisotropic particles nucleate simultaneously with random orientations and grow with constant velocities along their long and short axes [18]. In their work, the effects of blocking are only approximately accounted for, so that all particles which satisfy a relevant interaction geometry are potent blockers. The effects of blocker-blocker and higher-order interactions are ignored. When the particles are needlelike, our results indicate that this may be a rather severe approximation. To examine this claim, we solve Eq. (4) to first order in the ''blocking depth,'' excluding blocker-blocker and higher-order blocking effects. Under these conditions, $\widetilde{P}(x)$ has the form

$$\widetilde{P}(x) \approx 2\gamma I x e^{-\gamma I x^2}. \tag{11}$$

Equation (11) is a rather poor approximation to both Eq. (6) and the numerical data. For instance, Eq. (11) yields a distribution maximum which differs from that of the expression in Eq. (6) by 7.5%. It compares even more poorly with the numerical data, incurring an error of over 12% in the distribution maximum for the case of square lattice fragmentation. However, a solution of Eq. (4) to the next order in blocking depth yields a substantial improvement in the approximation, suggesting that higher-order corrections (blocker-blocker-blocker, etc.) do not have a significant effect on the crack length distribution function.

In short, we have developed approximate expressions for the ray and line length distribution functions for a general fragmentation process with heterogeneous nucleation of defects. The expressions we derived hold for arbitrary crack orientation distributions. Our results agree well with the existing numerical data and allow a systematic evaluation of the distribution moments for all cases. The lower-order moments are of interest experimentally, as one is often interested in the average crack length and variance for a given fragmentation process.

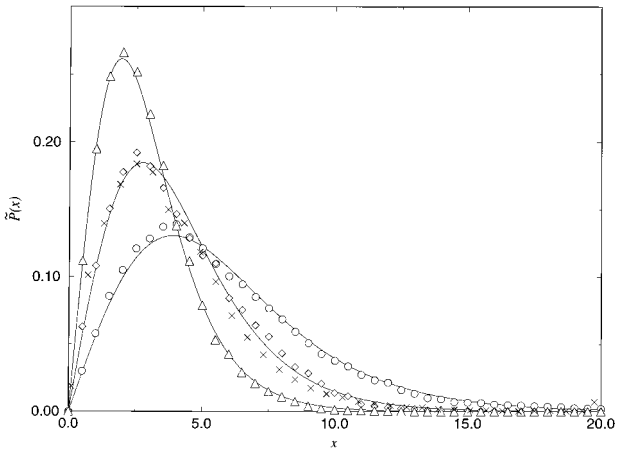

FIG. 11. Ray length probability distribution $\widetilde{P}(x)$ vs x. The solid lines are the mean-field solutions for $\gamma = 0.01$, 0.05, 0.10, and 0.20 with $D(\theta) = \frac{1}{3}[\delta(\theta) + \delta(\theta - \pi/3) + \delta(\theta - 2\pi/3)]$. Also plotted are the distributions obtained from simulations of the fragmentation model and the thin film fracture model ($\times$). The fracture simulations were carried out with the parameters $\gamma = 0.1$ and $\sigma_0 = 25.0$ on a lattice of size $L = 150$.

VII. COMPARISON OF THE MEAN-FIELD RESULTS WITH THE THIN FILM FRACTURE SIMULATIONS

To describe the ray length distribution obtained from the fracture patterns of our thin film model in the intermediate regime, $D(\theta)$ must have the form

$$D(\theta) = \tfrac{1}{3}[\delta(\theta) + \delta(\theta - \pi/3) + \delta(\theta - 2\pi/3)]. \tag{12}$$

Figure 11 shows a plot of the mean-field expression for $\widetilde{P}(x)$ vs x for $\gamma = 0.01$, 0.05, 0.10, and 0.20, with $D(\theta)$ given by Eq. (12). Also plotted in Fig. 11 are the normalized ray-length distributions obtained from averaging over 1000 simulations of the fragmentation model with $\gamma = 0.05$, 0.10, and 0.20. Finite size effects were eliminated by repeating the simulations on lattices of different sizes in order to obtain the limiting values of the data points as the lattice size tends to infinity. The latter are included to justify the mean-field approximation, as the agreement between the numerical and mean-field results is quite good. Finally, plotted in Fig. 11 is the normalized crack length distribution obtained from averaging over five fracture simulations with $\gamma = 0.1$. This distribution was generated by simulations on a lattice of size $L = 80$ with $\sigma_0 = 26.5$, within the intermediate regime. A finite size effect is discernible in the fracture data where the boundary increases the probability of obtaining shorter length cracks for defects near the edges of the film. Otherwise, the agreement is quite good over the entire range of crack lengths.

VIII. SUMMARY AND DISCUSSION

Lattice models are well suited to the simulation of fracture in bulk and have been employed to describe many of the generic features of stress relief in solids. Typically, these simulations rely on some method of relaxation about each configuration of cracks in the network as it sustains damage. The cracking is thus quasistatic and computationally inten-

sive. For this reason there are significant practical constraints on both the lattice size and geometry available to the researcher. In our simulations, cracking is dynamic, with no relaxation between incremental extensions of crack tips. The significant reduction in computation time allows us to be more realistic with the modeling. We employ a fully three-dimensional network and model the adhesive interaction between the substrate and film layer. We believe that the presence of an accurately modeled substrate is necessary for realistic film relaxation behavior. In our model the substrate applies a local traction at all points to a film which has a nonzero shear modulus. In Ref. [19] it is shown that the energy cost associated with shearing the film layer leads to qualitatively different crack morphologies in stochastic models of fracture. The same holds in deterministic fracture models as well [20].

We find that the long-time surface patterns emerging from our simulations can be classified broadly according to the complexity of the crack interactions. The three regimes we identify are distinguished by the applied stress. In the intermediate stress regime the complex crack tip interactions do not play a significant role in determining the final configuration of the surface cracks. This leads to the description of the fracture process in terms of a simple fragmentation model for which we have determined the crack length distribution function within a mean-field approximation.

The approximate crack length distribution functions derived in Sec. IV are applicable to generic fragmentation problems with simultaneous nucleation of cracks. Several examples of these appear in the literature with numerically estimated distribution functions. Our solution can be specialized to represent these models, and we find agreement with the numerical fits. Further, we have computed the moments of the general distribution functions.

ACKNOWLEDGMENTS

One of us (K.M.C.) acknowledges useful discussions with M. Mahadevan and M. P. Gelfand. This work was supported in part by NSF Grant No. DMR-9100257.

[1] S. Hansen and J. M. Ottino, Phys. Rev. E. **53**, 4209 (1996).
[2] P. Singh and M. K. Hassan, Phys. Rev. E. **53**, 3134 (1996).
[3] P. L. Krapivsky and E. Ben-Naim, Phys. Rev. E. **50**, 3502 (1994).
[4] M. H. Ernst and G. Szamel, J. Phys. A. **26**, 6085 (1993).
[5] R. M. Ziff, J. Phys. A. **25**, 2569 (1992).
[6] G. Baumann, M. Freyberger, W. G. Glöckle, and T. F. Nonnenmacher, J. Phys. A. **24**, 5085 (1991).
[7] See D. E. Grady and M. E. Kipp, J. Appl. Phys. **58**, 1210 (1985), and references therein.
[8] S. K. Shrinivasan, *Stochastic Theory and Cascade Processes* (American Elsevier, New York, 1969).
[9] J. Shinnar, J. Fluid Mech. **10**, 259 (1961).
[10] W. R. Johnson and C. C. Price, J. Polym. Sci. **45**, 217 (1960).
[11] H. K. Pulker, Thin Solid Films **89**, 191 (1982).
[12] J. M. Phillips, L. C. Feldman, J. M. Gibson, and M. L. McDonald, Thin Solid Films **107**, 217 (1983).
[13] J. J. Gilvarry, J. Appl. Phys. **32**, 391 (1961).
[14] M. A. Fortes and P. N. Andrade, J. Appl. Phys. **64**, 5157 (1988).
[15] P. A. Mulheran, Philos. Mag. Lett. **68**, 63 (1993).
[16] M. Rau, S. Sengupta, and H. K. Sahu, Phys. Rev. Lett. **75**, 2164 (1995).
[17] D. Zwillinger, *Handbook of Differential Equations* (Academic Press, New York, 1989).
[18] D. P. Birnie III and M. C. Weinberg, J. Chem. Phys. **103**, 3742 (1995).
[19] P. Meakin, in *Statistical Models for the Fracture of Disordered Media*, edited by H. J. Herrman and S. Roux (North-Holland, Amsterdam, 1990).
[20] K. Crosby and R. M. Bradley (unpublished).